Quantitative analysis of the structural health of railway turnouts using the acoustic emission technique

Kongpuang, Manwika; Culwick, Richard; Cheputeh, N-Asri; Marsh, Andrew; Jantara Junior, Victor L; Vallely, Patrick; Kaewunruen, Sakdirat; Papaelias, Mayorkinos

DOI:
10.1784/insi.2022.64.7.398

Document Version
Peer reviewed version

Citation for published version (Harvard):
Kongpuang, M, Culwick, R, Cheputeh, N-A, Marsh, A, Jantara Junior, VL, Vallely, P, Kaewunruen, S & Papaelias, M 2022, 'Quantitative analysis of the structural health of railway turnouts using the acoustic emission technique', *Insight: Non-Destructive Testing and Condition Monitoring*, vol. 64, no. 7, pp. 398-403. https://doi.org/10.1784/insi.2022.64.7.398

Quantitative Analysis of the Structural Health of Railway Turnout Using Acoustic Emission Technique

M. Kongpuang[1]*, R. Culwick[1], N. Cheputeh[1], A. Marsh[1], V. L. Jantara Junior[1], P. Vallely[1, 2], S. Kaewunruen[3], M. Papaelias[1]

[1]School of Metallurgy and Materials, The University of Birmingham, Birmingham, B15 2TT, UK
[2]Network Rail, Baskerville House, Birmingham, B1 2ND, UK
[3]School of Engineering, The University of Birmingham, Birmingham, B15 2TT, UK
(+44)7548799761
mxk763@student.bham.ac.uk

Abstract

Rail defects such as fatigue cracks have been one of the leading root causes of a number of derailments in the past. Using traditional NDT methods, cracks that initiate and propagate below the surface are difficult to detect at speed. Acoustic Emission (AE) is a more effective method for detecting and monitoring crack growth in rails online. This study investigates the applicability of AE for quantifying damage propagation in austenitic cast manganese steel used in manufacturing railway turnouts. The relationship between AE and crack growth rate in austenitic cast manganese steel samples fatigue tested in a three-point bending configuration was investigated by evaluating the AE activity with respect to Direct Current Potential Drop (DCPD) measurements and SEM fractography of the tested samples. From the results obtained, it was not possible to observe a clear relationship between AE activity and actual crack growth rate. Based on the SEM fractographic analysis this is likely due to the plasticity occurring at the tip of the fatigue crack in the tested samples. This is plausible since the cast manganese steel samples have been cut off from a plate, which has not been previously work-hardened. The effect of carbides present in the microstructure is an additional contributing factor. Further tests should be carried out on cast manganese steel samples that have been work-hardened prior to fatigue testing.

1. Introduction

At the turnout, the railhead is exposed to compressive rolling sliding loads as well as a heavy dynamic impact load. The load applied to this part of the track is more than the standard plain rails. As a result, austenitic cast manganese steel is required to be used due to its excellent mechanical properties. Cast manganese steel is a material that exhibits high work-hardening rate [1-2]. Carbides contribute to the overall strength exhibited by the material. There are three ways that inclusions, such as MnS can act as crack initiators. High stress concentrations in the centre of elongated inclusions, such as MnS, could induce interfacial debonding, whilst brittle inclusions can crack [3]. Cracks that begin and propagate below the surface are difficult to detect with traditional NDT methods. Therefore, Acoustic Emission (AE) is a more appropriate method for crack growth monitoring because since the elastic stress waves released from the crack tip can be detected by piezoelectric sensors [4]. AE can monitor cracking from the initiation

stage up to final failure. Experiments using AE to detect fatigue crack initiate and propagation in alloys undergoing cyclic loading in laboratory test have been reported previously [16].
Several papers have studied the relationship between AE count rate and ΔK for steel and welded steel specimens outside of the rail industry context, showing an approximately linear relationship on a logarithmic scale [5]. In 3-point bending experiments, the relationship between the crack propagation mechanism and AE signals was investigated, and the failure phenomenon was interpreted by evaluating the amplitude distribution, AE event count, and total AE energy [6]. As measured against loading cycles in rail steel inspection, the cumulative signal amplitude and duration showed a similar trend to crack length. Both the energy duration rates of AE demonstrated a related dependence on ΔK through a Paris-Erdogan type power law [7].

2. Material

2.1 Material characterisation

Before 3-point bending fatigue tests were carried out, chemical composition and microstructural analysis were performed on samples in order to determine the chemical composition of the studied steel, as shown in Table 1.

Table 1. Typical chemical composition Austenitic cast manganese steel (in wt %).

Carbon	Silicon	Manganese	Phosphorous	Sulphur
1.20%	0.15%	11.00-14.00%	0.02%	0.02%

A scanning electron microscope was used to examine the microstructure. To obtain contrast between the different phases identified in this type of material, a Marble etching agent was used as etchant. The microstructure of austenitic cast manganese steel consists of austenite and small carbides along the grain boundary as shown in Figure 1.

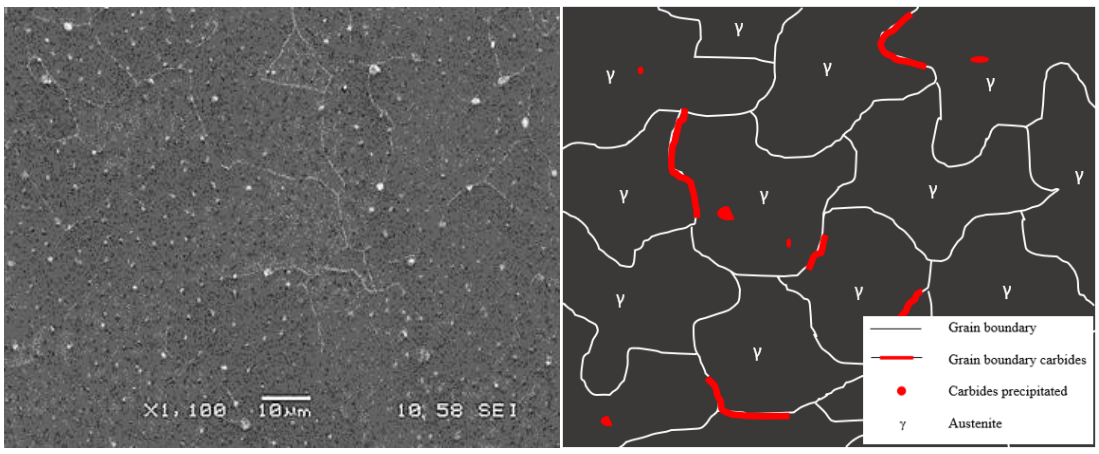

Figure 1. SEM micrographs of the metallographic samples and schematic of austenitic microstructure showing austenite phase, grain boundary, and carbide precipitation in the grain.

X-ray powder diffraction was performed in this study using Bruker D8 Advance, employing a Cu Kα (λ = 1.5406 Å) anode with Ni filters. Following Bragg's law, each dot in the diffraction pattern above forms from the constructive interference of X-rays passing through a crystal. Figure 2 shows the XRD phase analysis results for a sample of austenitic cast manganese, which show that austenite is the dominant phase present in the sample, confirming the microscopy result previously explained. The primary carbide formed in the sample, Fe, Mn_3C, can also be seen in the peak.

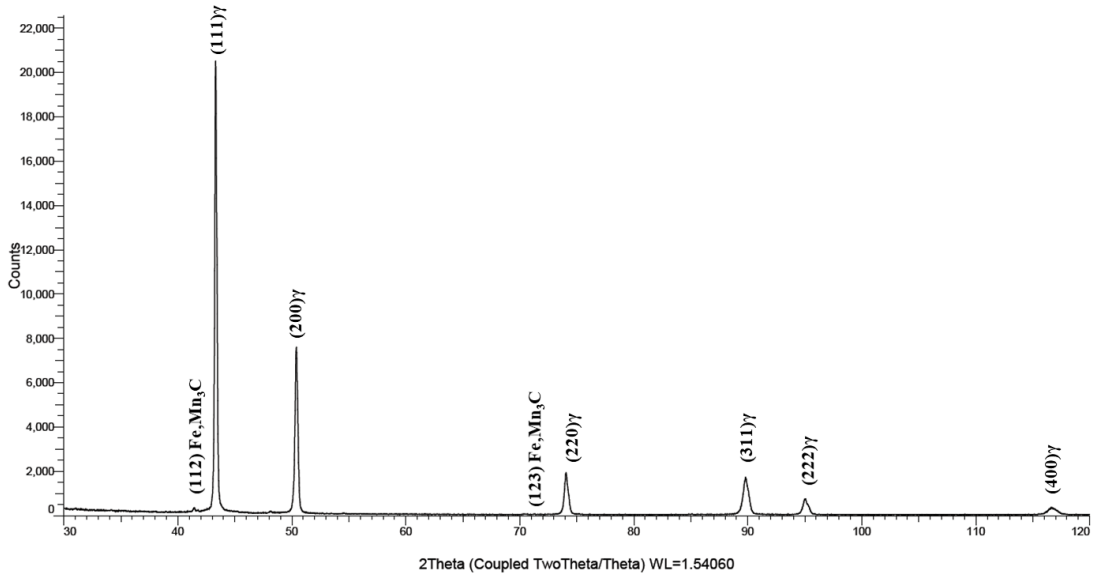

Figure 2. X-ray diffraction patterns of tested of austenitic cast manganese steel.

2.2 Specimens

A plate of austenitic cast manganese steel was procured from West Yorkshire Steel. Each material was plasma cut to produce ten samples of dimensions 120 mm x 20 mm x 10 mm (L x H x W) suitable for fatigue testing. A notch with depth 2 mm and 30^o angle was spark eroded in each sample tested (Figure 3). The samples were pre-cracked using a vibrophore electro-mechanical high-frequency fatigue machine to an initial crack length of 3-4 mm. approximately.

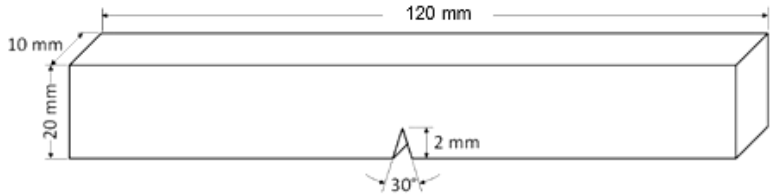

Figure 3. Single edge-notch specimen extraction in a three-point bending test.

2.3 Pearson Correlation and Linear Regression Analysis

A correlation or simple linear regression may be used to determine if there is a relevant linear relationship between two numeric variables. Correlation analysis provides details with respect the strength and direction of the linear relationship between two variables. In comparison, in a linear equation, simple linear regression analysis predicts parameters that estimate one values of a variable depending on the other [14]. The Pearson correlation coefficient can be interpreted as shown in Table 2.

Table 2. A conventional approach to interpreting a correlation coefficient (R) [15]

Guidelines for interpreting Pearson correlation coefficient (R)	**Interpretation**
0.00 - 0.10	Negligible correlation
0.10 – 0.39	Weak correlation
0.40 – 0.69	Moderate correlation
0.70 – 0.89	Strong correlation
0.90 – 1.00	Very strong correlation

3. Experimental Procedure

3.1 Pre-cracking method and measurement

Each sample was pre-cracked using an Amsler 20KN vibrophore electro-mechanic high-frequency fatigue machine. A cyclic load of 0.65 kN - 6.5 kN (R = 0.1) was applied to the sample in a 3-point bending configuration using a sinusoidal wave pattern with an estimated frequency of 85 Hz, and 70 dB was set as the AE threshold. The use of metallographic replicas observed through an optical microscope confirmed pre-cracking. Using ImageJ software, the initial crack length was measured from the surface to the tip of the cracks, including the spark wire eroded notch [8].

3.2 Cyclic Three-Point Bending test

A force of 0.45 kN – 4.5 kN, was subsequently applied under constant amplitude sinusoidal wave loading at a frequency of 5 Hz and a fixed stress ratio (R= 0.1). A commercial PAC AE system employing two R50α piezoelectric sensors connect to a 2/4/6 pre-amplifier were used to record the AE activity. Sampling rate was set at 5 MSPS, with peak Definition Time at 600 µs, Hit Definition Time at 1000 µs, and Hit Lockout Time at 2000 µs. The AE amplifier is set at 40 dB while the minimum threshold is set at 50 dB, changed down from 70 dB for pre-cracking for greater sensitivity. The fatigue crack propagation was monitored in parallel using a DCPD instrument**.**

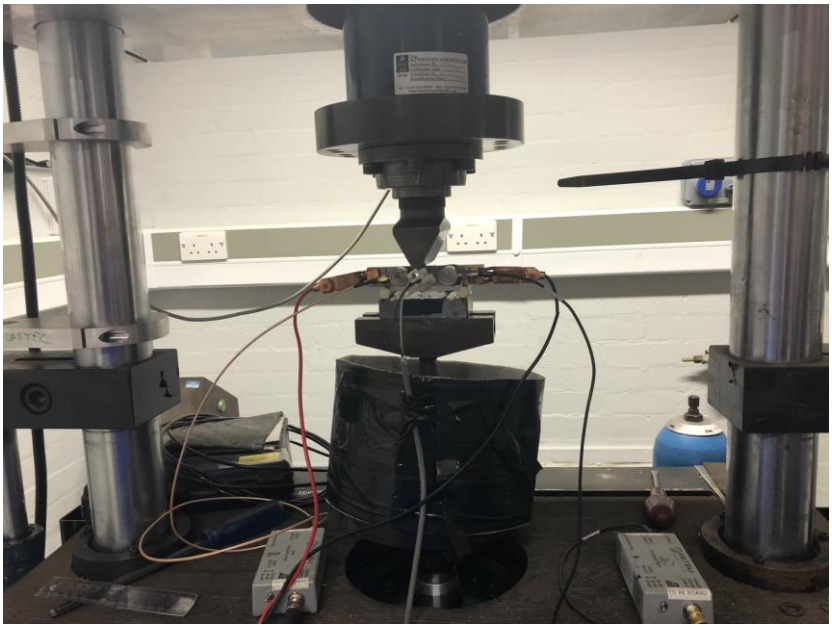

Figure 4. Cyclic Three-point-bending test.

The fundamental operational concept of the AE-based damage detecting technique is shown in Figure 5.

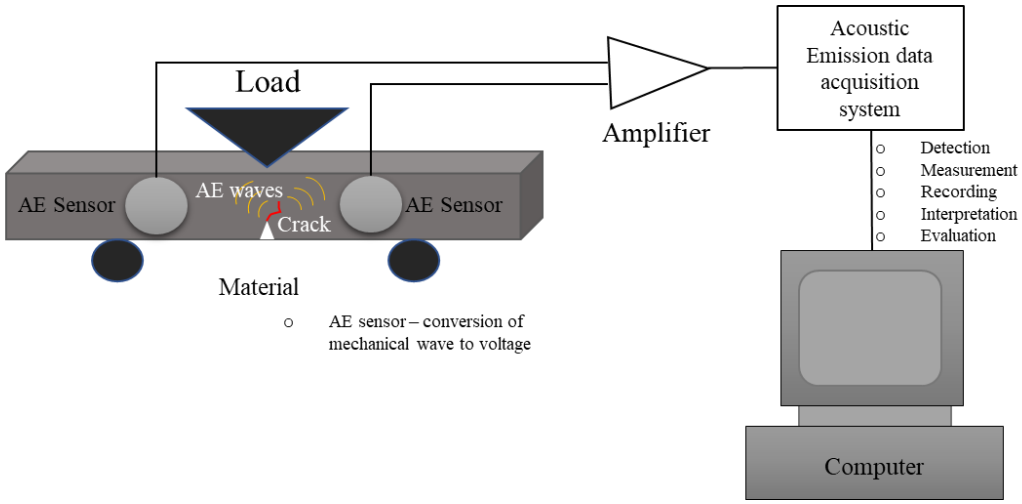

Figure 5. Scheme of the acoustic emission system for the identification of damage.

3.3 Direct Current Potential Drop (DCPD)

In laboratory experiments, the direct current potential drop (DCPD) method was used to measure the length of cracks during fatigue crack growth. On the chart recorder, the pen traces can reflect the crack length increase. Johnson's formula can be used to calculate the crack length [9].

$$\frac{V(a)}{V(a_0)} = \frac{\arccos h\left[\frac{\cosh(\pi y/2W)}{\cos(\pi a/2W)}\right]}{\arccos h\left[\frac{\cosh(\pi y/2W)}{\cos(\pi y/2W)}\right]} \quad \text{.....(1)}$$

Johnson's formula can be obtained by solving

$$a = \frac{2W}{\pi}\cos^{-1}\frac{\cosh\left(\frac{\pi y}{2W}\right)}{\cosh\left\{\left(\frac{V_a}{V_{a_0}}\right)\cosh^{-1}\left[\cosh\left(\frac{\pi y}{2W}\right)/\cos\left(\frac{\pi a_0}{2W}\right)\right]\right\}} \quad \text{.....(2)}$$

Where a_o is the initial crack length, $V(a_o)$ is the corresponding potential, W represents the specimen width, and y represents the distance of electrodes from the potential probe to the crack mouth.

During the stable crack propagation, also referred to as the Paris regime, the crack growth rate da/dN is the power function of the SIF range leading to the well-known Paris equation. The fatigue crack growth curve relates to the crack growth rate (da/dN) to the stress intensity factor range applied [10].

$$\frac{da}{dN} = C\Delta K^m, or: \log\left(\frac{da}{dN}\right) = \log C + m\log\Delta K \quad \text{.....(3)}$$

The crack length da/dN is the crack growth rate, C and m are constants that particular on the material, environment, stress ratio, and ΔK range from the stress intensity factor during the fatigue cycle.

$$\Delta K = K_{\max} - K_{\min} \quad \text{.....(4)}$$

For a specific geometry, K_I coefficients are defined [10]

$$K_I = \frac{4P}{B}\sqrt{\frac{\pi}{W}}\left[1.6\left(\frac{a}{W}\right)^{\frac{1}{2}} - 2.6\left(\frac{a}{W}\right)^{\frac{3}{2}} + 12.3\left(\frac{a}{W}\right)^{\frac{5}{2}} - 21.2\left(\frac{a}{W}\right)^{\frac{7}{2}} + 21.8\left(\frac{a}{W}\right)^{\frac{9}{2}}\right] \text{.....(5)}$$

The applied load is the thickness of the specimen, a the crack length, and W is the width of the specimen.

3.3 SEM images

The crack surfaces of all samples were opened with a Charpy test hammer and cut to roughly 5mm x 10mm x 20 mm for microscopy. The SEM was performed using the JEOL6060 system to analyse the physical characteristics of test specimens and analyse the elemental composition of an area of interest on the samples with Energy Dispersive X-Ray Spectroscopy (EDS) used to determine elemental composition.

4. Results and Discussion

4.1 AE signal analysis

Both sensors in austenitic cast manganese steel generally follow the same pattern. The energy of the AE signal grows steadily in early crack propagation but rapidly at failure in samples 1 and 3, which corresponds to the crack progression from initiation to propagation during the fatigue test. Other samples, such as samples 4 and 6, demonstrate that the energy of AE signals increases steadily at first, meaning that the AE signals detected at this stage are generated purely by the plastic zone formation before the crack tip [12].

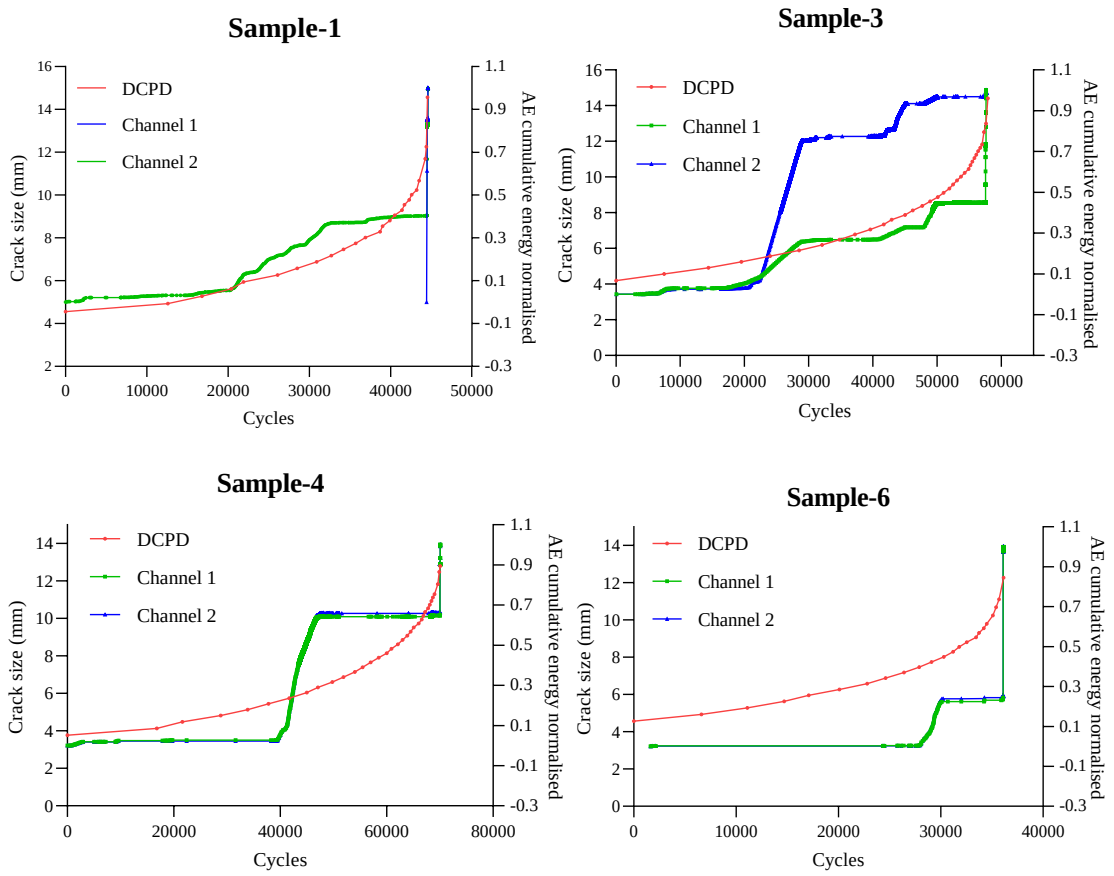

Figure 6. A cumulative AE energy plot from R50α Sensors compares to the crack size measured using the DCPD instrument of austenitic cast manganese steel samples 1, 3, 4, and 6.

Plotting amplitude against fatigue cycles helps show this difference in activity more clearly, with only short peaks of AE activity in early crack propagation ending with a high peak at failure, as opposed to more continuous activity.

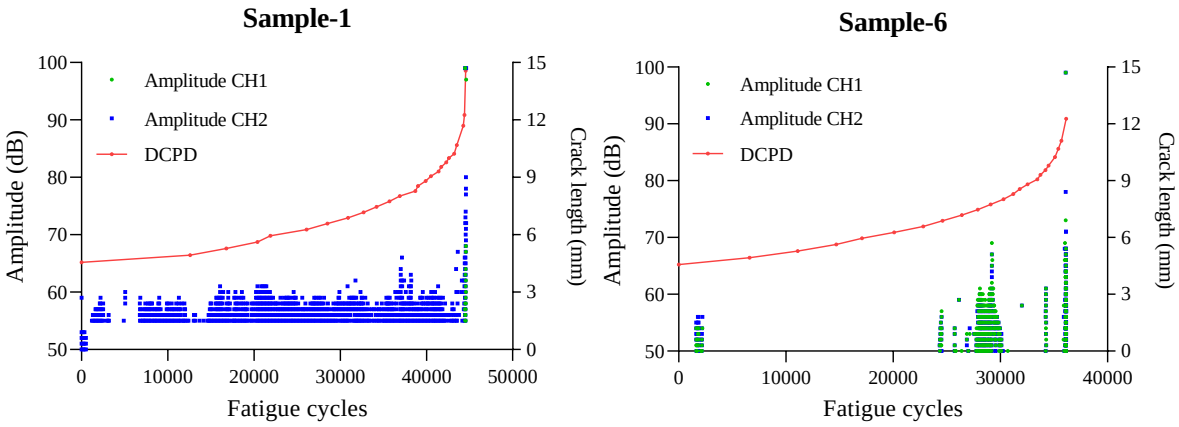

Figure 7. Amplitude against fatigue cycles for austenitic cast manganese steel sample 1 (continuous crack activity) and sample 6 (short peaks in early – ending with a high peak at failure).

4.2 Fatigue crack growth rate

According to the test standard ASTM E647, 1990 [17], the experiment was conducted using cyclic load under constant amplitude loading. The relationship between crack size (*a*) and cycle (*N*) is the primary data collected from the experiment. Then use the data obtained to calculate and plot the relationship between fatigue crack growth rates (*da/dN*) and crack-tip stress-intensity factor range (*ΔK*).

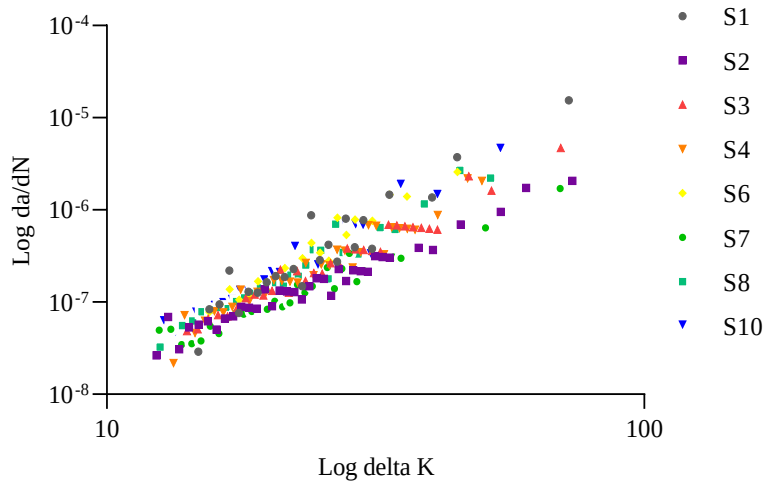

Figure 8. The Paris law for fatigue crack growth rates of austenitic cast manganese steel (Stage II in Micro-mechanism of Fatigue).

After the plotted plot *log da/dN* as a function of *log ΔK*, the slope of the plot would give the *m*, and the *Y-intercept* will provide the value of *C*. The average *C* and *m* values from the experiment in austenitic cast manganese steels are $C = 4.08 \times 10^{-11}$, and $m = 2.604$ *with* $R = 0.972$, *and* $R^2 = 0.945$.

4.3 AE and crack growth parameters

The crack growth rate and the energy rate were calculated in the same way. As a result, the energy rate and ΔK relationship can be defined as follows (and similarly for Amplitude rate- *dA/dN*, Count rate- *dC/dN*, and Duration rate- *dD/dN*).

$$\frac{dE}{dN} = C\Delta K^{m}, or: \log\left(\frac{dE}{dN}\right) = \log C + m\log\Delta K$$

Figure 9 show the crack growth rate with parameters rate and ΔK in the logarithmic scale austenitic cast manganese samples on a logarithmic scale. The average *C* and *m* values from the experiment are shown in Table 3.

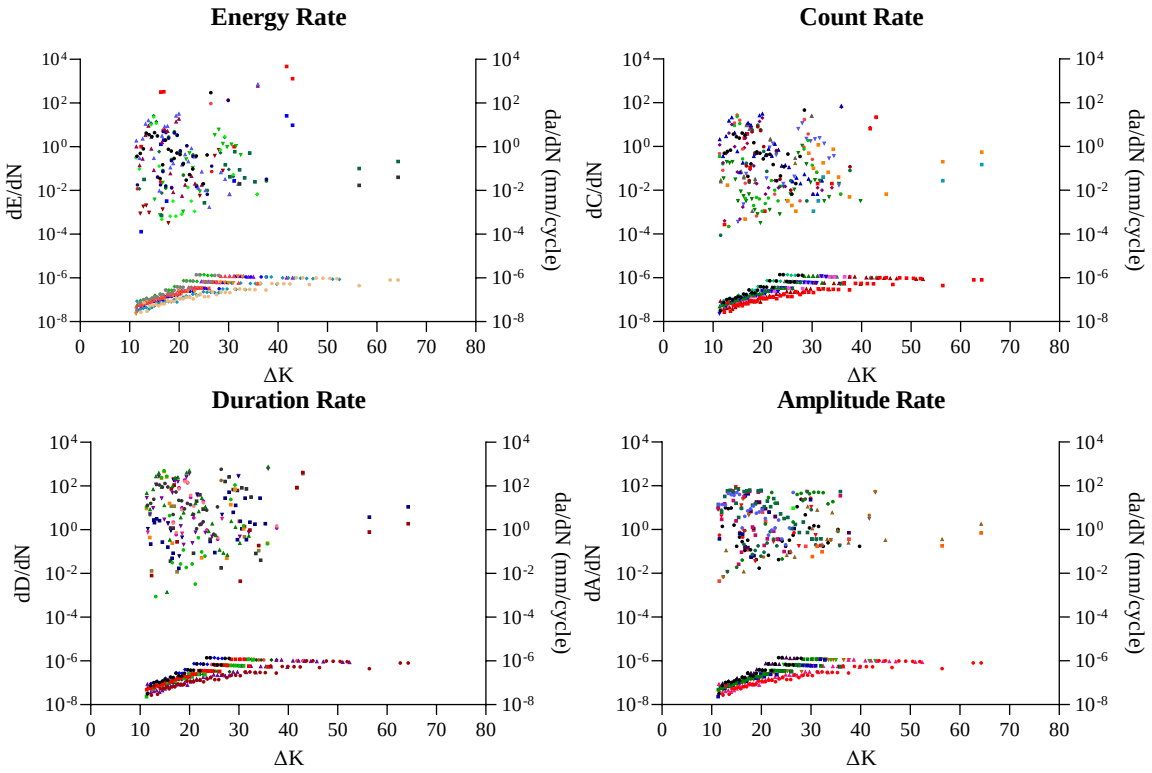

Figure 9. The crack growth rate parameters with ΔK for all austenitic cast manganese steel samples in logarithmic scale.

Table 3. Average fit parameters against ΔK

AE Parameters	C	m	R	R^2	Interpretation
Energy rate	2.53 x10^{-2}	0.917	0.139	0.019	Weak correlation
Duration rate	4.24 x10	0.013	0.036	0.001	Negligible correlation
Count rate	5.47 x10^{-3}	1.079	0.107	0.011	Negligible correlation
Amplitude rate	1.14 x10	0.182	0.005	0.000	Negligible correlation

The AE data did not fit well with the Paris law trend. This is attributed to plasticity, since the samples had not been work-hardened and the plate is in the as-received condition. This expected to be less of an issue in actual cast manganese crossings which have been work-hardened and will not exhibit much plasticity. It has been proposed that samples are work-hardened so a new set of tests is carried out to evaluate the effect of work-hardening on AE activity during fatigue testing.

4.4 Fracture Surface Analysis

After completing the cyclic 3-point fatigue bending tests, the fracture surfaces of austenitic cast manganese steels were examined under a microscope. Figure 10 shows micrographs of the fractured surface of the sample in different areas.

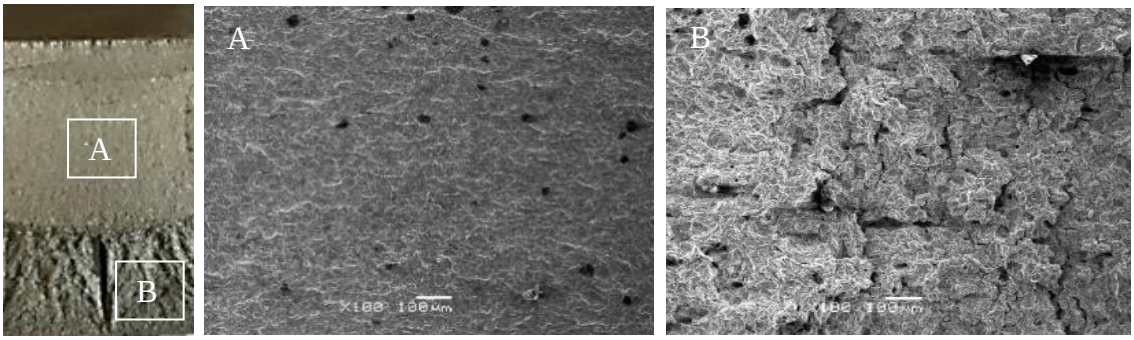

Figure 10. Macroscopic view of the fractured surface showing the morphologies of the fatigue crack growth area (A) and fast fracture area (B).

This hypothesis of plasticity is supported by SEM analysis of austenitic cast manganese steel fracture surfaces. The presence of a ridge and ductile tearing can be seen in the microstructure of the fatigue area of crack growth in the samples. This also relates to austenitic cast manganese steel, which helps understand why elastic waves emit no energy. Microstructural analysis of samples 4 and 6, which showed very little AE activity only with a few jumps in energy before failure, reveals large groupings of inclusions in the microstructure, which are especially visible at regions along the crack length corresponding to rapid increase in accumulated energy. The relative absence of carbides throughout the microstructure is related to more elastic processes in samples 1 and 3, meaning that the relative absence of carbides throughout the microstructure is linked to more elastic processes. One conclusion drawn from these findings is that the carbide distribution is just as significant as its presence. Scattered inclusions may allow more plastic deformation in crack growth, while high-concentration regions may result in more elastic behaviour as the crack is forced to pass through inclusions, resulting in a brittle fracture.

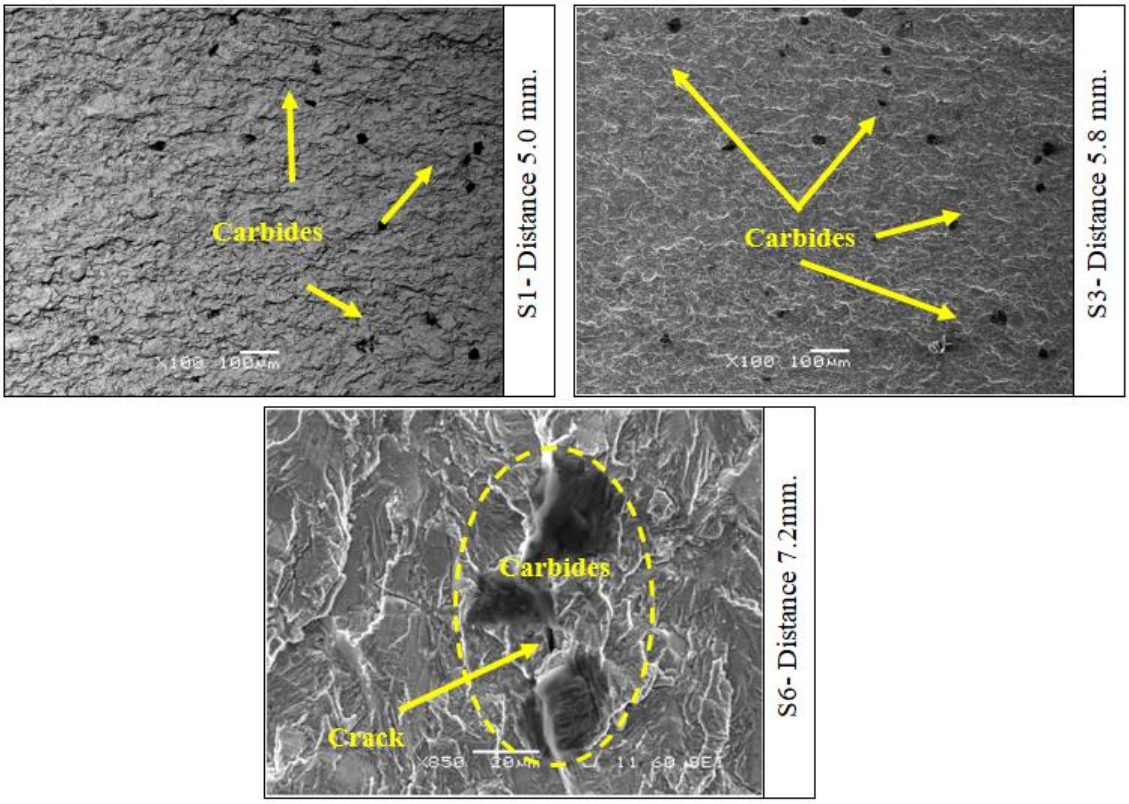

Figure 11. SEM Micrographs show the fracture surface (top left) scatter of carbides of sample 1 at a distance of 5.0 mm. (top right) scatter of carbides of sample 3 at approximately 5.8 mm crack length, and (bottom) carbides and crack under carbides of sample 6 at approximately 7.2 mm crack length.

Plastic deformation occurs in all cases, resulting in the formation of cracks. The crack usually begins at the surface, where the loads are highest. After initiation, most cracks are limited to the plastically deformed layer following the weakest links in the microstructures, which is a weaker non-twinned grains steel. Various processes can produce AE during plastic deformation, but in twin growth observed in austenitic cast manganese steel, the signal strength is negligible [13].

4. Conclusion and Future work

Three-point bending fatigue tests were carried out on cast manganese steel samples. Crack growth was monitored using a commercial AE system procured from PAC. From the results obtained, it was impossible to observe a clear Paris trend from the recorded AE activity. Based on hardness measurements and the SEM fractographic analysis this is likely to be due to the plasticity occurring at the tip of the fatigue crack in the tested samples. This is possible because the austenitic cast manganese steel samples were cut from a plate that had not been work-hardened previously and an additional contributing factor is the effect of carbides in the microstructure before fatigue testing, further studies should be performed on cast manganese steel samples that have been work-hardened and then be carried out using the AE monitoring techniques used in this study on the live network.

Acknowledgements

The financial support from the Thai government and EPSRC with respect to this work is gratefully acknowledged.

References

1. Dastur YN, Leslie WC. Mechanism of work hardening in Hadfield manganese steel. Metallurgical Transactions A. 1981;12(5):749-759.
2. Bayraktar E, Khalid FA, Levaillant C. Deformation and fracture behaviour of high manganese austenitic steel. Journal of Materials Processing Technology. 2004;147(2):145-154.
3. Liu, C., Bassim, M. and Lawrence, S. S. (1993) 'Evaluation of fatigue-crack initiation at inclusions in fully pearlitic steels', Materials Science and Engineering: A, 167(1-2), pp. 107-113.
4. Ph Papaelias, M., Roberts, C. and Davis, C. (2008) 'A review on non-destructive evaluation of rails: state-of-the-art and future development', Proceedings of the Institution of Mechanical Engineers, Part F: Journal of Rail and rapid transit, 222(4), pp. 367-384.
5. Marfo, A., Luo, Y. and Zhong-an, C. (2013) 'Quantitative acoustic emission fatigue crack characterisation in structural steel and weld', Advances in Civil Engineering, 2013.
6. Yoneda, K. and Ye, J. (2006) 'Crack propagation and acoustic emission behavior of silver-added Dy123 bulk superconductor', Physica C: Superconductivity and its applications, 445, pp. 371-374.
7. Shi, S., Han, Z., Liu, Z., Vallely, P., Soua, S., Kaewunruen, S. and Papaelias, M. (2018) 'Quantitative monitoring of brittle fatigue crack growth in railway steel using acoustic emission', Proceedings of the Institution of Mechanical Engineers, Part F: Journal of Rail and Rapid Transit, 232(4), pp. 1211-1224.
8. Schindelin, J., Arganda-Carreras, I., Frise, E., Kaynig, V., Longair, M., Pietzsch, T., Preibisch, S., Rueden, C., Saalfeld, S. and Schmid, B. (2012) 'Fiji: an open-source platform for biological-image analysis', Nature methods, 9(7), pp. 676.
9. Johnson, H. J. M. R. and Standards (1965) 'Calibrating the electric potential method for studying slow crack growth', 5(1), pp. 442-445.
10. Paris, P. and Erdogan, F. J. J. o. b. e. (1963) 'A critical analysis of crack propagation laws', 85(4), pp. 528-533.
11. ASTM, E. (2007) 'Standard Test Methods for Notched Bar Impact Testing of Metallic Materials'
12. Wang, W.-F. and Wu, M.-J. (2006) 'Effect of silicon content and aging time on density, hardness, toughness and corrosion resistance of sintered 303LSC–Si stainless steels', Materials Science and Engineering: A, 425(1-2), pp. 167-171.
13. Máthis, K. and Chmelík, F. (2012) 'Exploring plastic deformation of metallic materials by the acoustic emission technique', Acoustic Emission, pp. 23-48.
14. Mindrila, D. and Balentyne, P. (2017) 'Scatterplots and correlation', Retrieved from. Montgomery, D. C., Peck, E. A. and Vining, G. G. (2021) Introduction to linear regression analysis. John Wiley & Sons.
15. Schober, P., Boer, C. and Schwarte, L. A. (2018) 'Correlation coefficients: appropriate use and interpretation', Anesthesia & Analgesia, 126(5), pp. 1763-1768.

16. Aggelis, D., Kordatos, E. and Matikas, T. (2011) 'Acoustic emission for fatigue damage characterization in metal plates', Mechanics Research Communications, 38(2), pp. 106-110.
17. ASTM, E. (2011) '647: Standard test method for measurement of fatigue crack growth rates', Annual book of ASTM standards, 3, pp. 591-630.